Pergamon

Transport-controlled kinetics of dissolution and precipitation in the sediments under alkaline and saline conditions

NIKOLLA P. QAFOKU,* CALVIN C. AINSWORTH, JAMES E. SZECSODY, and ODETA S. QAFOKU

Pacific Northwest National Laboratory, Richland, Washington 99352 USA

Abstract—Over 1.6 million liters of radioactive, high-temperature, Al-rich, alkaline and saline high-level waste (HLW) fluids were accidentally discharged from tank leaks onto the sediments at the Hanford Site, Washington. In order to better understand processes that might occur during the migration of HLW through sediments and to estimate their extents, we studied the effects of Al-rich, alkaline and saline solutions on soil mineral dissolution and precipitation during reactive transport. Metal- and glass-free systems were used to conduct miscible-displacement experiments at 50 °C under CO_2 and O_2 free conditions. Results showed significant release of Si, K, Al, Fe, Ca, Mg, and Ba into the aqueous phase. The transport-controlled release of these elements was time dependent as evidenced by its extent varying with the fluid residence time. Silica initial dissolution rates (6.08×10^{-11} and 5.38×10^{-13} mol m^{-2} s^{-1}) increased with base concentration, decreased with Al concentration, and decreased with fluid residence time. Aluminum precipitation rates varied in the range from 0.44 to 1.07×10^{-6} mol s^{-1} and were faster in these column experiments than in previous batch studies. The initial rate constant of Al precipitation reaction was 0.07 h^{-1} (half-life of 9.9 h at about 3 PV); it increased up to 0.137 h^{-1} (half-life of 5.1 h at about 20 PV). The precipitates identified with SEM and suggested from the modeling results were mainly NO_3-cancrinite. SEM analyses also indicated the formation of sodalite when Al was not present in the leaching solution. In addition, results from modeling suggested the precipitation of brucite, goethite and gibbsite; the latter may precipitate in the presence of high Al concentrations. Aqueous and solid phase transformations caused by base-induced dissolution and subsequent secondary phases precipitation should be important determinants of the fate of contaminants and radionuclides in the vadose zone under alkaline and saline conditions.   *Copyright © 2004 Elsevier Ltd*

1. INTRODUCTION

Nuclear weapons production has resulted in the generation of significant amounts of high-level radioactive waste (HLW) at Department of Energy (DOE) sites. At the Hanford Site, Washington, the liquid waste was stored in 177 underground tanks, 67 of which had or were suspected to have leaked. Of particular interest is the liquid waste that leaked from the *S-SX* tanks containing the self-boiling HLW, which was Al-rich, hyperalkaline and saline fluids with concentrations of $Al(OH)_4^-$, NaOH and $NaNO_3/NaNO_2$ as high as 3.66, 5 and more than 10 mol L^{-1}, respectively. Substantial quantities of ^{137}Cs, ^{60}Co, ^{90}Sr, ^{99}Tc, ^{234,238}U, and Cr were also present in these fluids (Jones et al., 2000; Serne et al., 2002).

Between 1.92 and 3.46 million liters of waste fluids were deposited to the underlying vadose zone, creating a variety of environmentally-related problems. The effects of these Al-rich, hyperalkaline and saline solutions in the liquid and solid phase transformations in the sediments are not well studied.

The soil minerals in these sediments may undergo base-induced dissolution when they react with alkaline solutions (Serne et al., 2002; Qafoku et al., 2003b). The dissolution reaction follows a more favorable path in the presence of a catalyst, such as OH. The adsorption of OH to surface sites proximal to the metal weakens the Al-O bond strength of the Al-O-Si structural groups (Ganor and Lasaga, 1998) and hydrolysis of aluminosilicates increases in basic pHs (Chou and

Wollast, 1985; Knauss and Wolery, 1989; Brady and Walther, 1992; Hellmann, 1994; Blum and Stillings, 1995; Walther, 1996).

On the other hand, Al in the aqueous phase decreases the aqueous OH concentration because it forms aluminate, which is the dominant Al aqueous species at alkaline pH. Aluminate may also inhibit base-promoted dissolution because it competes with OH for surface sites, decreasing OH surface concentration (Ganor and Lasaga, 1998). Under either steady state, or far from equilibrium conditions, dissolution rates at constant pH for albite (Oelkers et al., 1994), K-feldspars (Gautier et al., 1994), kaolinite (Devidal et al., 1997), and basaltic glass (Oelkers and Gislason, 2001) exhibited inverse relationships to the aqueous Al concentration.

In addition to dissolution, precipitation of secondary minerals may occur in the sediment exposed to HLW liquids (Qafoku et al., 2003a). Minerals in the groups of zeolite, sodalite, and cancrinite were formed in Al and Na-rich hyperalkaline systems (Buhl and Lons, 1996; Gerson and Zheng, 1997; Zheng et al., 1997; Barnes et al., 1999a; Barnes et al., 1999b; Buhl et al., 2000; Bickmore et al., 2001; Qafoku et al., 2003a). Cancrinite and sodalite are feldspathoids with identical chemical formula ($Na_8Al_6Si_6O_{24}X_2$), where X can be ½ CO_3, ½ SO_4, Cl, OH, or NO_3 (Barnes et al., 1999a). They have a molar Si:Al ratio of 1:1. In similar NO_3-rich systems, nitrate-sodalite (Buhl and Lons, 1996) and nitrate-cancrinite (Bickmore et al., 2001; Qafoku et al., 2003a) were also formed.

The previous batch studies conducted with high pH and ionic strength (IS) solutions showed that these systems were very dynamic, i.e., the properties of the solid and liquid phases were

---

* Author to whom correspondence should be addressed (nik.qafoku@pnl.gov).

Table 1. Selected physical properties in each column.

Column ID	Pore volume cm³	Water content cm³ cm⁻³	Residence time h	Bulk density g cm⁻³	Flow rate cm³ min⁻¹	Mass of the sediments (at the end of experiments)[b] g
1	43.15	0.37	8.05	1.59	0.0893 (77)[a]	179.95
2	52.11	0.44	8.46	1.48	0.1050 (121)	183.88 (−7.68)[c]
3	52.94	0.45	8.37	1.45	0.1054 (152)	170.01 (−7.67)
4	22.07	0.44	4.08	1.50	0.0901 (132)	75.75 (+2.13)
5	44.37	0.38	23.56	1.65	0.0314 (270)	192.90 (+13.14)
6	44.51	0.38	8.20	1.65	0.0905 (185)	192.52 (+11.4)
7	48.86	0.41	8.53	1.55	0.0954 (80)	180.91 (+3.51)
8	47.45	0.41	32.48	1.58	0.0243 (183)	184.66 (+2.69)
9	45.67	0.41	7.90	1.62	0.1008 (188)	189.42 (+1.39)
10	20.99	0.42	4.98	1.56	0.0703 (173)	78.61 (+1.65)

[a] The average flow rate was calculated from experimental measurements (the number in parentheses).

[b] Pore volume, water content, residence time and bulk density were calculated based on the sediment mass at the end of experiment.

[c] The sediment mass at the end of experiments was different from that initially packed in the columns (mass differences in grams are presented in parentheses).

changing continuously because of dissolution and precipitation (Bickmore et al., 2001; Qafoku et al., 2003a; Qafoku et al., 2003b). But because the sediment/water ratio in batch experiments is quite different than that present in the vadose zone sediments, the best way to study the dynamics of these changes at field-scale sediment/water ratios is with miscible-displacement experiments.

The current research was undertaken to quantify coupled dissolution and precipitation reactions that may occur during transport of Al-rich, highly alkaline and saline solutions. The coupling of geochemical and transport processes in flowing systems often manifests effects that are not generally present in batch systems. For this reason, a series of miscible displacement experiments were conducted at 50 °C under CO_2 and O_2 free conditions. Thermodynamically stable, Al-rich, hyperalkaline and saline solutions were used to leach the sediments packed in columns. To separate the contrary effects of base catalysis and the apparent inhibition of Al on dissolution and precipitation reactions, different leaching fluids were used to leach the columns. The release in the effluents of major elements that compose the soil matrix, such as Si, Fe, K, Al, Ca, Mg, Ba, Mn was followed throughout the experiments. Parameters of the dissolution and precipitation kinetics were calculated based on these experimental data. In addition, Field Emission Scanning Electron Microscopy (FESEM) and Energy-Dispersive X-Ray Spectroscopy (EDS) were used to characterize the posttreatment sediments and newly formed precipitates. These data provided a set of useful scientific information on how flow affects the extent of dissolution and precipitation in the sediments under extreme conditions of alkaline pH and high IS.

2. MATERIAL AND METHODS

2.1. Sediments

The silty coarse sand sediment was collected at approximately 7 m depth in the Environmental Restoration Disposal Facility (ERDF) pit in the Hanford 200E area, while the fine sandy silt sediment was collected at approximately 13 m depth in the Navy submarine reactor core pit in the Hanford 200E area. The two sediments were from the same geologic formation (Hanford formation, 30 to 40 m thick in this location), deposited by the same fluvial process, and differ only slightly in grain size. The two pits were 5 miles apart and on the south and north sides of the 200E area. The bottom of the tanks was about 6 to 8 m depth. To work with a representative sediment of the vadose zone where radionuclide migration occurred from the 200E tanks, a composite sample of the two sediments (50/50 on a weight basis) was used in the experiments reported in this paper.

The mineralogy of the bulk composite sample was the following: plagioclase feldspars, quartz, biotite, K-feldspars, smectite, chlorite, amphibole, calcite, magnetite, hematite, and laumontite (Serne et al., 2002). The <1.5 μm fraction was dominated by smectite, plagioclase, biotite, K-spars, quartz, and chlorite. Iron oxides were detected only in trace amounts on some mica surfaces during the SEM analysis; Fe was mainly incorporated in clay minerals, such as smectite, chlorite and biotite, (Serne et al., 2002).

2.2. Column Experiments

Saturated miscible displacement experiments were used to study dissolution and precipitation reactions during reactive transport of the Al-rich, hyperalkaline and saline fluids in the Hanford sediments. Aluminum hydroxides, NaOH and $NaNO_3$ were three of the principal electrolyte components present in the waste tanks at the Hanford Site, and the $Al(OH)_4^-$-NaOH-$NaNO_3$-H_2O system should be considered as the simplest chemical system that represents the more complex mixed electrolyte fluids present in the tanks.

Ten polyvinyl chloride (PVC) columns with inner diameter of 2.4 or 3.2 cm and length of 9.5 or 14.5 cm were packed uniformly with the composite sediments (~8% water content) by pouring 10-g increments into the columns, then tamped with a plastic dowel. Before adding the next increment, the surface of the tamped portion was lightly scratched to minimize layering inside columns.

Filter papers (0.25 cm thick and 10 μm pore diameter) were used at the top and bottom of each column to assist in uniform distribution of the leaching solution at the column inlet and to prevent sediments from being removed from or blocking the column outlet and tubing that connected the column outlet with the syringe pumps. An ion chromatograph pump with Delrin- and Teflon-wetted parts controlled flow through the columns that were oriented vertically inside a water bath at 50 °C. All leaching solutions were prepared in a CO_2 and O_2 free glove box and were kept inside well-sealed 3L plastic bottles. The atmosphere inside these bottles was continuously saturated with helium gas during the experiments.

The column effluent was collected in sealed helium flushed 60 mL septa-top plastic bottles with approximately 20 mL of degassed DI-water to immediately dilute the effluent and avoid precipitation when they cooled to room temperature. When physical and chemical steady-state conditions were established the flow interruption method (Reedy et al., 1996; Brusseau et al., 1997) was used in some columns to test if nonequilibrium conditions were affecting solute transport. Selected physical properties of each packed column were presented in Table 1.

FESEM and EDS analyses were conducted in the sediments at the

end of different columns. A LEO 982 FESEM system with an Oxford ISIS energy dispersive X-ray microanalysis system, with a Si-Li detector was used for scanning electron microscopy and EDS analyses. This instrument is an ultra high-performance scanning electron microscope with a resolution of 1 nm at 30 kV and 4 nm at 1 kV. We used the microanalysis system to do both qualitative and quantitative elemental analyses of the secondary minerals that were formed during the experiment and to identify the soil minerals onto which these secondary phases precipitated.

2.3. Solutions

Before the onset of displacement experiments, soil columns were slowly saturated and leached with degassed DI-water for approximately 5 pore volumes (PV) to fully saturate the available pore space inside the columns. The columns were then leached with the respective solutions presented in Table 2. Because Cr was present in high concentrations in the waste tank fluids at the Hanford Site, some of the solutions were also rich in Cr(VI). The results of Cr(VI) behavior in these systems were presented in another paper (Qafoku et al., 2003c). Aqueous effluent concentrations of Al, Si, K, Mg, Ca, Ba, Cr, Mn, and Fe were determined using a Perkin Elmer Optima 3000DV inductively coupled plasma atomic emission spectroscopy (ICP-AES). Instrument detection limits were: 5, 3, 4, 70, 0.1, 0.1, 0.1, 0.4 μg L^{-1} for Al, Fe, Si, K, Mg, Ca, Ba, and Mn, respectively.

2.4. Chemical Speciation Modeling

Data from these experiments were modeled using GMIN, which is a chemical equilibrium program that uses a free energy minimization approach (Felmy, 1995). The free-energy models incorporated in GMIN include the Pitzer equations to calculate the excess free energy of an aqueous electrolyte solution. This code may be successfully used to model data from our experiments conducted with hyperalkaline and hyperasaline solutions. We used GMIN for speciation purposes, as well as to calculate the activity coefficients for the aqueous species and the saturation indexes of different secondary phases that might precipitate during the experiments.

The following solid phases that may be formed during these experiments were considered in the simulations: $NaNO_3$ (solid), brucite ($Mg(OH)_2$), portlandite ($Ca(OH)_2$), quartz (SiO_2), SiO_2 (amorphous), gibbsite ($Al(OH)_3$), goethite ($FeOOH$), low OH nitrate-cancrinite, and high OH nitrate-cancrinite ($Na_8Si_6Al_6O_{24}(NO_3)_2 \cdot 4H_2O$). The thermodynamic constants of formation of cancrinite were taken from the literature of Bickmore et al. (2001). Although the thermodynamic constant of formation of hydroxyl-sodalite ($Na_8Si_6Al_6O_{24}OH_2 \cdot 2H_2O$) was reported in the literature (Park and Englezos, 1999; Bickmore et al., 2001), this information was not available for nitrate-sodalite, so this solid phase was excluded from these simulations.

2.5. Sediment Dissolution

The dissolution reaction of the sediments treated with Al-rich, hyperalkaline and saline fluids may be written as follows:

Sediments (biotite, chlorite, quartz, feldspar. . .) + OH + Na

$$+ NO_3 + Al = Si + Al + K + Fe + \ldots \ldots \quad (1)$$
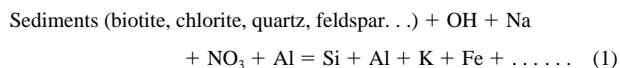
Taking Si as an example, the rate expression for the release of Si may be written:

$$\begin{aligned}
\delta Si/\delta t = &\{k_{OH\text{-}biotite}[OH]^a + k_{Na\text{-}biotite}[Na]^b + k_{NO3\text{-}biotite}[NO_3]^c \\
&+ k_{Al\text{-}biotite}[Al]^d\} + \{k_{OH\text{-}chlorite}[OH]^e + k_{Na\text{-}chlorite}[Na]^f \\
&+ k_{NO3\text{-}chlorite}[NO_3]^g + k_{Al\text{-}chlorite}[Al]^h\} + \{k_{OH\text{-}quartz}[OH]^i \\
&+ k_{Na\text{-}quartz}[Na]^j + k_{NO3\text{-}quartz}[NO_3]^k \\
&+ k_{Al\text{-}quartz}[Al]^l\} + \{k_{OH\text{-}feldspar}[OH]^m + k_{Na\text{-}feldspar}[Na]^n \\
&+ k_{NO3\text{-}feldspar}[NO_3]^o + k_{Al\text{-}feldspar}[Al]^p\}\ldots \quad (2)
\end{aligned}$$

The dissolution rates were calculated using the finite difference method as follows:

$$d[Si]/dt = \{[Si]_t - [Si]_0\}/t\} \quad (3)$$

In expression [3] t is the fluid residence time inside the column, $[Si]_t$ is the Si concentration in the soil solution (mol L^{-1}) at a specific time during leaching. In our experiments, the columns were initially saturated with DI-water, and $[Si]_0$ was measured in the effluent samples (at least 3 measurements per column) collected at the column outlet at the very beginning of the leaching experiments, when an effluent volume of less than ½ PV was collected at the column outlet. In these experiments, the Si concentration in the soil solution at the onset of dissolution varied between 0.69 and 1.52 mmol L^{-1} in different columns. The rate of dissolution in mol m^{-2} s^{-1} was calculated based on the mass of the sediments packed in each column, the volume of one PV and the EGME (ethylene glycol mono-ethyl ether) surface area of the pretreatment sediment (51.28 m^2 g^{-1}).

Silicon concentration in the effluent at the onset of precipitation may be used as $[Si]_t$ to calculate the initial rate of dissolution in different columns. In addition, Si concentration at different times during leaching may be used as $[Si]_t$ to calculate the apparent rate of dissolution in different columns and at different times during leaching. Both dissolution and precipitation may simultaneously occur in these column experiments, when the aqueous phase is oversaturated with respect to different secondary precipitates. The amount of Si that remains in the aqueous phase and appears in the effluents during leaching is, therefore, the difference between Si released upon soil mineral dissolution and Si removed from the aqueous phase because of precipitation. For this reason, all dissolution rates that are calculated based on Si concentration in the effluent at different times during leaching, with the exception of the rates calculated before or at the onset of precipitation, should be considered as apparent dissolution rates.

2.6. Secondary Phases Precipitation Rate

The first-order kinetic model was applied to the data collected from these column experiments with different fluid residence times, to calculate the rate constants of the precipitation reactions based on the changes in Al concentration in the soil aqueous phase. The integrated form of that model is:

$$[A]/[A]_0 = \exp(-kt) \quad (4)$$

where the [A] is Al concentration at time t, $[A]_0$ is the initial Al concentration, k is the rate constant for the precipitation reaction, and t is the fluid residence time. The log of this equation can be taken as (Brezonik, 1993):

$$\log[A] - \log[A]_0 = \log(e^{-kt}) \quad (5)$$

or

$$\log[A] = -0.434kt + \log[A]_0 \quad (6)$$

A plot of log [A] vs t should yield a straight line for reactions following first-order kinetics. The rate constant is obtained from the slope, $k = -2.3 \times (\text{slope})$. The reaction half-life was calculated as follows:

$$t_{1/2} = 0.693/k \quad (7)$$

The rate of precipitation (mol s^{-1}) is calculated with data collected from the columns leached with Al-rich, alkaline and saline solutions, based on Al concentration in the input solution and Al concentration in the effluent at different times during leaching.

3. RESULTS

3.1. The Catalytic Effect of Base on Dissolution

3.1.1. Si, K, Fe, and Al releases in the effluents

Numerous observations made during these experiments clearly showed that base induced dissolution occurred in the sediments treated with alkaline solution. Dissolution did not occur when the sediments packed in column 1 were leached with a dilute sodium chromate solution (0.192 mmol L^{-1} Cr) at

Table 2. Initial and apparent dissolution rates based on Si release into the aqueous phase.

Column ID and leaching solutions[a]	Si concentration mol/L	Diss. rate mol m^{-2} sec^{-1}	Pore volume	Experimental time h
Column 2 1 mol L^{-1} NaOH and	0.17149	24.64×10^{-12}	1.19	10.12
0.192 mmol L^{-1} Cr[b]	0.05894	8.33×10^{-12}	3.90	33.01
	0.04907	6.90×10^{-12}	5.58	47.19
	0.04811	6.76×10^{-12}	7.50	63.43
	0.04089	5.72×10^{-12}	9.93	84.04
	0.03084	4.26×10^{-12}	18.50	156.51
	0.01794	2.39×10^{-12}	42.70	361.28
Column 3 4 mol L^{-1} NaOH and	0.30348	60.86×10^{-12}	1.04	8.70
0.192 mmol L^{-1} Cr	0.15016	29.97×10^{-12}	3.01	25.19
	0.10966	21.81×10^{-12}	5.33	44.61
	0.08584	17.02×10^{-12}	8.37	70.06
	0.06767	13.36×10^{-12}	11.03	92.32
	0.03528	6.83×10^{-12}	20.08	168.07
	0.02677	5.12×10^{-12}	27.59	230.93
	0.01377	2.50×10^{-12}	46.21	386.77
Column 4 1 mol L^{-1} NaOH and	0.14728	56.48×10^{-12}	1.45	5.92
0.055 mol L^{-1} Al[c]	0.01024	3.49×10^{-12}	3.43	13.99
	0.01481	5.25×10^{-12}	5.96	24.32
	0.01102	3.79×10^{-12}	7.47	30.48
	0.00876	2.92×10^{-12}	11.84	48.31
	0.00260	0.53×10^{-12}	20.75	84.66
	0.00237	0.44×10^{-12}	28.13	114.79
	0.00175	0.20×10^{-12}	43.29	176.62
	0.00162	0.15×10^{-12}	50.58	206.37
	0.00139	0.00×10^{-12}	62.44	254.75
Column 5 1 mol L^{-1} NaOH, 0.055	0.24564	12.92×10^{-12}	1.63	38.40
mol L^{-1} Al and 1.923 mmol	0.02328	1.16×10^{-12}	3.5	82.46
L^{-1} Cr	0.05292	2.73×10^{-12}	5.08	119.68
	0.05966	3.09×10^{-12}	6.06	142.77
	0.05075	2.61×10^{-12}	8.5	200.26
	0.03659	1.86×10^{-12}	10.98	256.69
	0.02476	1.24×10^{-12}	15.04	354.24
	0.01046	0.48×10^{-12}	20.2	475.91
	0.00291	0.09×10^{-12}	31.82	749.68
Column 6 1 mol L^{-1} NaOH, 0.055	0.15608	23.62×10^{-12}	1.38	11.32
mol L^{-1} Al and 1.923 mmol	0.00942	1.23×10^{-12}	3.55	29.11
L^{-1} Cr	0.01211	1.64×10^{-12}	5	41
	0.01494	2.07×10^{-12}	8.5	69.7
	0.00838	1.07×10^{-12}	11	90.2
	0.00620	0.74×10^{-12}	15.14	124.15
	0.00296	0.24×10^{-12}	20	164
	0.00214	0.12×10^{-12}	37	303.4
	0.00025	0.00×10^{-12}	65.35	535.87
Column 7 1 mol L^{-1} NaOH, 0.055	0.12972	22.13×10^{-12}	1.45	12.36
mol L^{-1} Al and 0.192 mmol	0.01510	2.47×10^{-12}	2.22	18.93
L^{-1} Cr	0.00773	1.21×10^{-12}	8.68	74.04
	0.00413	0.59×10^{-12}	11.46	97.75
	0.00244	0.30×10^{-12}	20.48	174.69
	0.00206	0.06×10^{-12}	27.26	232.52
Column 8 1 mol L^{-1} NaOH, 0.055	0.24697	10.53×10^{-12}	1.4	45.47
mol L^{-1} Al and 0.192 mmol	0.04118	1.71×10^{-12}	4.66	151.36
L^{-1} Cr	0.05331	2.23×10^{-12}	6.07	197.15
	0.04500	1.87×10^{-12}	8.48	275.43
	0.03922	1.63×10^{-12}	11.1	360.53
	0.03658	1.51×10^{-12}	15.17	492.72
	0.01351	0.52×10^{-12}	20.02	650.25
	0.00734	0.26×10^{-12}	23.26	755.48
	0.00200	0.03×10^{-12}	27.79	902.62
	0.00225	0.04×10^{-12}	30.84	1001.68
Column 9 1 mol L^{-1} NaOH, 0.165	0.09078	14.82×10^{-12}	1.74	13.75
mol L^{-1} Al and 0.192 mmol	0.00269	0.36×10^{-12}	3.94	31.13
L^{-1} Cr	0.00271	0.27×10^{-12}	5.2	41.08
	0.00268	0.62×10^{-12}	6.18	48.82
	0.00241	0.22×10^{-12}	8.37	66.12
	0.00181	0.18×10^{-12}	11.07	87.45
Column 10 1 mol L^{-1} NaOH and	0.00274	0.54×10^{-12}	8.45	42.08
0.165 mol L^{-1} Al	0.00237	0.43×10^{-12}	11.36	56.57
	0.00128	0.14×10^{-12}	20.4	101.59
	0.00060	0.17×10^{-12}	40.47	201.54

[a] the background solution in all columns was 1 mol L^{-1} NaNO$_3$.
[b] as Na$_2$CrO$_4$ · 4H$_2$O.
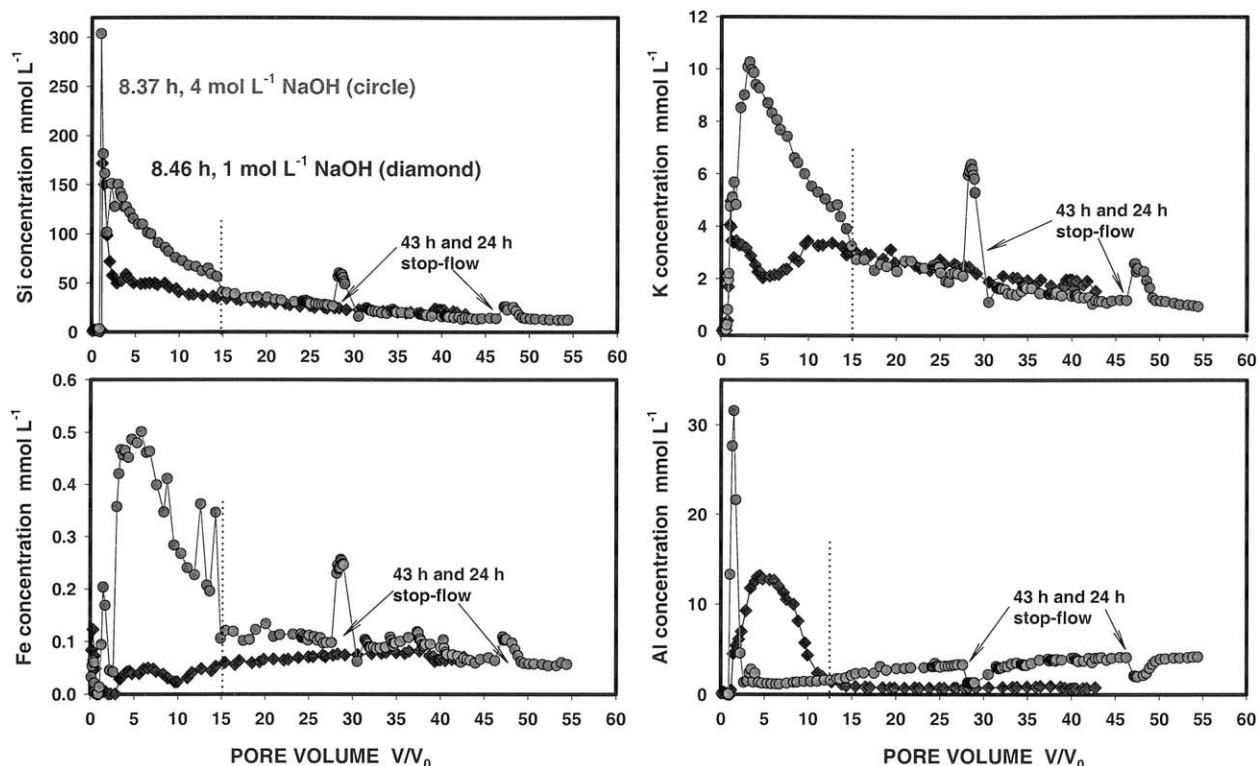[c] as Al(NO$_3$)$_3$ · 9H$_2$O.

Fig. 1. Changes in Si, Fe, K, and Al concentration with time in columns 2 and 3 (fluid residence time of 8.46 and 8.37, respectively). Both columns were leached with 1 mol L^{-1} $NaNO_3$ solutions that were 1 mol L^{-1} and 4 mol L^{-1} in NaOH, respectively.

circumneutral pH, and the effluent Si concentration was constant at 1.42 mmol L^{-1}. The addition of 1 and 4 mol L^{-1} NaOH resulted in large Si releases from the sediments, which peaked at ~ 1PV, then decreased (Fig. 1.) Silicon concentration in the effluents of column 2 (1 mol L^{-1} OH) reached a maximum of approximately 170 mmol L^{-1} at 1.19 PV, while in column 3 (4 mol L^{-1} OH) a peak Si concentration of ~300 mmol L^{-1} was observed at 1.04 PV.

The initial dissolution rate was greater in the 4 mol L^{-1} than in the 1 mol L^{-1} NaOH leaching experiment at the beginning of the second PV (Table 2). In addition, the apparent dissolution rates measured at 6 PV were also greater in the 4 mol L^{-1} than in the 1 mol L^{-1} NaOH column (Table 2). However, similar apparent dissolution rates were observed at later times (>15 PV) when similar amounts of Si were released in the effluents of both columns.

Base concentration also affected the K release into the aqueous phase upon dissolution of K-bearing soil minerals. Similar trends of K concentration with time were observed in the 4 mol L^{-1} OH and 1 mol L^{-1} OH columns in the first 1.5 PV, and a K concentration of ~5 mmol L^{-1} was observed in the effluents of both columns (Fig. 1). However, the trends diverged in the following 3 PV (a peak concentration of 10.26 mmol L^{-1} was observed in the 4 mol L^{-1} OH column), converged at approximately 15 PV, and followed similar decreasing slopes for the rest of experiment. More K was released in the effluents of the 4 mol L^{-1} OH column in the first 15 PV, but as in the case of Si, the base effect on K release vanished at 15 PV.

Much more Fe was released in the effluent of the column

leached with the 4 mol L^{-1} NaOH solution, and a peak concentration of 0.5 mmol L^{-1} was observed at 5.77 PV (Fig. 1). Iron concentration in the effluent steadily decreased afterwards, and reached a similar value to the one observed in the column leached with the 1 mol L^{-1} NaOH column at 30 PV. In contrast, an increasing trend in the Fe concentration with time was observed in the first 40 PV in the 1 mol L^{-1} OH column; Fe concentration appeared to have reached a steady-state plateau in both columns, which occurred after 40 PV.

Aluminum reached a peak concentration of 31.6 mmol L^{-1} at 1.47 PV in the column that was leached with the 4 mol L^{-1} OH solution, but immediately decreased to a concentration of 1.33 mmol L^{-1} at 2.62 PV. An increasing trend of Al concentration with time was observed afterwards. Aluminum concentration in the effluent of the 1 mol L^{-1} OH column increased gradually until it peaked at 13.17 mmol L^{-1} (4.48 PV); it reached a value of approximately 0.7 mmol L^{-1} at 15 PV, and did not change much for the duration of the experiment. Aluminum mass released in the effluent was greater in the 1 mol L^{-1} than in the 4 mol L^{-1} OH column in the first 12 PV. However, more Al was released into the effluents of the 4 mol L^{-1} OH column after 12 PV.

3.1.2. Results from applying the stop-flow technique

The stop-flow technique was used to investigate whether equilibrium conditions were established in these column experiments. Different durations of stop-flows were applied to mea-
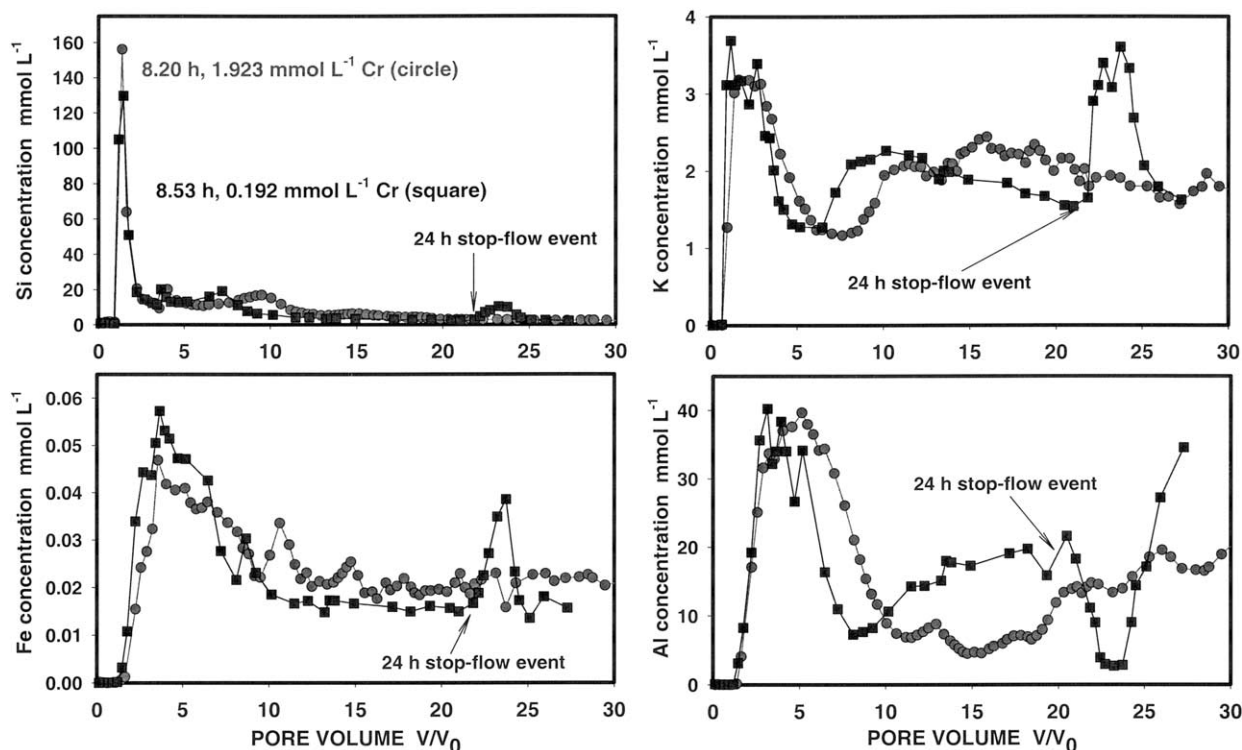
Fig. 2. Changes in Si, Fe, K, and Al concentrations with time in columns 6 and 7, which had similar fluid residence time (8.20 and 8.53 h). Both columns were leached with 1 mol L^{-1} NaNO$_3$, 1 mol L^{-1} NaOH, and 0.055 mol L^{-1} Al(NO$_3$) solutions that were 1.923 and 0.192 mmol L^{-1} in Cr, respectively.

sure the direction and extent of time-dependent processes. The 43 and 24 h stop-flows revealed nonequilibrium conditions in the 4 mol L^{-1} OH column; Si concentration in the contact solution more than doubled (from 26.8 to 56.5 mmol L^{-1}) during the 43 h stop-flow at 27.5 PV, and also increased from 13.8 to 25.7 mmol L^{-1} during the 24 h stop-flow applied later at 46.2 PV. The apparent dissolution rates, however, decreased during the stop-flow events (from 5.12×10^{-12} mol m^{-2} s^{-1} measured before the stop-flow at 27.5 PV to 1.30×10^{-12} mol m^{-2} s^{-1}, and from 2.50 to 0.83×10^{-12} mol m^{-2} s^{-1} at 46.2 PV).

Significant increases in effluent K and Fe concentrations were observed during both stop-flow events applied in the 4 mol L^{-1} OH column. In sharp contrast, Al concentration decreased significantly during these stop-flow events.

3.1.3. Results from modeling

Results from modeling with GMIN showed that solution became immediately supersaturated in column 2 (1 mol L^{-1} OH) with respect to high OH nitrate-cancrinite and brucite at 1.19 PV. If all Fe released is considered to be only Fe(III), goethite might have also precipitated from this solution. The aqueous phase remained saturated with respect to high OH nitrate-cancrinite, brucite and goethite at 20.98 and 40.01 PV. The predominant Al aqueous species was Al(OH)$_4^-$ while the predominant Si aqueous species were H$_2$SiO$_4^{2-}$, H$_3$SiO$_4^-$, Si$_2$O$_3$(OH)$_4$, and CaH$_2$SiO$_4$. Aluminum appeared to control the rate of cancrinite precipitation under these con-

ditions, where aqueous Si concentration was much greater than that of Al.

As it was expected, the results from modeling were different in column 3 (4 mol L^{-1} OH), although the same predominant aqueous Al and Si species were present in the effluent of this column. The solution became immediately saturated with respect to cancrinite, brucite, and goethite at 1.04 PV, and remained saturated with respect to these three solid phases at 20.08 and 45.5 PV.

3.2. The Effect of Cr Concentration on Dissolution and Precipitation

The presence of Cr in the leaching solution had little effect on dissolution. Similar releases of Si, K, Fe, and Al into the aqueous phase were observed in the effluent of columns 6 and 7, which had similar fluid residence times but were leached with the 1.923 and 0.192 mmol L^{-1} Cr solutions, respectively (Fig. 2). They had similar initial and apparent dissolution rates (Table 2). In addition, the amounts of Si, K, Fe, and Al released in the effluents of these columns in the first liter of effluent collected at column's outlet were also similar (11.695 and 11.118 mmol Si, 2.013 and 1.923 mmol K, 0.024 and 0.023 mmol Fe, and 15.078 and 16.998 mmol Al, respectively). Even though the amount of Al that precipitated in column 6 was slightly greater than that in column 7, the average Al precipitation rates were similar (Table 3).

Table 3. Apparent and average precipitation rates based on Al removal from the aqueous phase (standard deviations are given in parentheses; n is the number of rate measurements considered in the calculations of the average precipitation rates).

Column ID	Pore volume	Time H	Prec. rate mol sec^{-1} (per kg solution)	Average precipitation rate mol sec^{-1} (per kg solution)
Column 4	3.4	13.99	1.000×10^{-6}	1.069×10^{-6} ($\pm 0.278 \times 10^{-6}$, n = 8)
	5.2	21.37	0.693×10^{-6}	
	6.5	26.60	0.787×10^{-6}	
	11.8	48.26	1.076×10^{-6}	
	20.7	84.62	1.565×10^{-6}	
	30.0	122.48	1.329×10^{-6}	
	43.3	176.62	1.095×10^{-6}	
	50.6	206.37	1.006×10^{-6}	
	62.4	254.75	0.928×10^{-6}	
Column 5	3.3	77.51	0.472×10^{-6}	0.573×10^{-6} ($\pm 0.057 \times 10^{-6}$, n = 9)
	4	94.24	0.518×10^{-6}	
	5	117.8	0.573×10^{-6}	
	6	141.36	0.577×10^{-6}	
	8.5	200.26	0.592×10^{-6}	
	11	259.16	0.621×10^{-6}	
	15	353.4	0.643×10^{-6}	
	20	471.2	0.632×10^{-6}	
	31	730.36	0.505×10^{-6}	
Column 6	3.2	26.57	0.667×10^{-6}	0.976×10^{-6} ($\pm 0.501 \times 10^{-6}$, n = 9)
	4	32.8	0.549×10^{-6}	
	5	41	0.454×10^{-6}	
	6	49.2	0.651×10^{-6}	
	8.5	69.7	1.219×10^{-6}	
	11	90.2	1.620×10^{-6}	
	15	123	1.697×10^{-6}	
	20	164	1.389×10^{-6}	
	71	582.2	0.538×10^{-6}	
Column 7	2.7	22.86	0.610×10^{-6}	1.048×10^{-6} ($\pm 0.371 \times 10^{-6}$, n = 8)
	5.2	44.01	0.610×10^{-6}	
	6	51.18	1.220×10^{-6}	
	8.5	72.50	1.514×10^{-6}	
	11	93.83	1.290×10^{-6}	
	20	170.6	1.045×10^{-6}	
	23	196.19	0.440×10^{-6}	
Column 8	3.5	113.68	0.422×10^{-6}	0.437×10^{-6} ($\pm 0.019 \times 10^{-6}$, n = 8)
	5.9	190.98	0.422×10^{-6}	
	6	194.88	0.417×10^{-6}	
	8.5	276.08	0.422×10^{-6}	
	11	357.28	0.441×10^{-6}	
	15	487.2	0.462×10^{-6}	
	20	649.6	0.459×10^{-6}	
	23	747.04	0.454×10^{-6}	
Column 9	4	31.6	1.018×10^{-6}	1.075×10^{-6} ($\pm 0.238 \times 10^{-6}$, n = 7)
	5	39.5	0.816×10^{-6}	
	6	47.4	0.793×10^{-6}	
	8.5	67.15	1.063×10^{-6}	
	11	86.9	1.286×10^{-6}	
	20	158	1.458×10^{-6}	
	40	316	1.094×10^{-6}	
Column 10	20	167.4	1.018×10^{-6}	1.018×10^{-6} ($\pm 0.001 \times 10^{-6}$, n = 2)
	60	502.2	1.019×10^{-6}	

3.3. The Effect of Fluid Residence Time on Dissolution and Precipitation

3.3.1. Si, K, and Fe releases in the effluents

Increased contact time of alkaline solution with sediments resulted in increased concentration of leached ions, but the actual dissolution rates decreased. It appears that dissolution is coupled with precipitation reactions which remove additional mass in the longer residence time columns, resulting in less apparent dissolution. Columns 5 and 6 were leached with identical solutions, but different fluid residence time regimes were applied to them (23.56 and 8.20 h, respectively) (Fig. 3). Because the presence of Cr in the leaching solution was shown to have little effect on the extent of dissolution and precipitation, data from column 4, with fluid residence time of 4.08 h, were also included in Figure 3 to compare them with those of columns 5 and 6. Much more Si was released in the first 30 PV in the slow-flow column 5, and less Si was released in the faster columns 4 and 6, with respective fluid residence times of 4.08 and 8.20 h. The initial dissolution rate decreased considerably
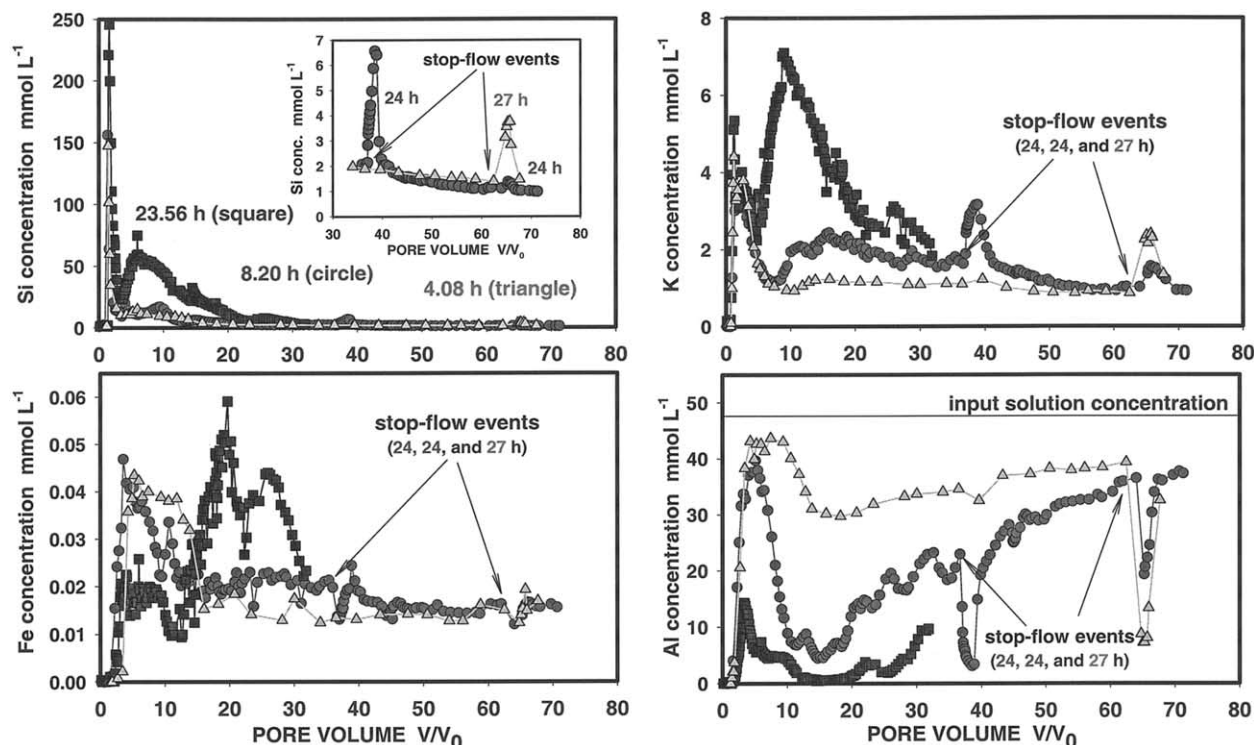
Fig. 3. Changes in Si, Fe, K, and Al concentrations with time in columns 4, 5, and 6. They were leached with 1 mol L^{-1} NaNO$_3$, 1 mol L^{-1} NaOH, and 0.055 mol L^{-1} Al(NO$_3$) solutions that were 0, 1.923 and 1.923 mmol L^{-1} in Cr, respectively. Different fluid residence time regimes were applied to these columns (4.08, 23.56, and 8.20 h, respectively).

with the fluid residence time (Table 2), but similar apparent dissolution rates were observed afterwards and the residence time effect on Si release vanished after approximately 30 PV.

It is interesting to notice here that even though the values of the peak Si concentrations were quite similar, more Si was released in the effluent of column 2 than in the effluent of column 6; the former was leached with an Al-free, alkaline solution. The initial dissolution rates in these columns were similar (Table 2), but the apparent dissolution rate at ~9 PV was greater in column 2 than in column 6.

Similar fast releases of K were observed in all columns in the first PV (Fig. 3), which most likely were the result of exchange reactions of K for Na that was present in the leaching solution in a significant concentration (2 mol L^{-1}). The release of K in column 5 and 6 followed similar trends in the subsequent 2 to 3 PV, but the trends diverged at 5.5 PV, and much more K was released in the slow-flow column afterwards. Even less K was released in the effluent of column 4 (Fig. 3).

Aqueous Fe concentration was also affected by the fluid residence time, but in a different way (Fig. 3). More Fe was released in the first 12 PV in the effluents of columns 4 and 6 with respective fluid residence times of 4.08 and 8.2 h, as compared to the amount released in column 5 (fluid residence time of 23.56). A reversed picture was observed after 12 PV, and much more Fe was released in the slow-flow column from 12 to 32 PV. The Fe concentration in the effluents of both columns 4 and 6 reached an apparent steady state at approximately 0.015 mmol L^{-1} after ~45 PV.

3.3.2. Al release in the effluents

Aluminum was added in the input solutions used to leach columns 4, 5 and 6. In these experiments, a significant Al attenuation was observed confirming that Al was participating in the formation of secondary phases. Aluminum concentration in the short-residence time column 4 reached a maximum value of $C/C_0 = 0.85$ (46.75 mmol L^{-1}/55 mmol L^{-1}) after approximately 7.5 PV, decreased afterwards towards a minimum concentration of less than 30 mmol L^{-1} at ~15 PV, and started to increase towards the value of the input solution in the subsequent PVs (Fig. 3). The same trend was observed in column 6, although much more Al was precipitating in this column. Aluminum was removed to a greater extent in the slow-flow column (column 5). In this column, Al concentration peaked at 3.4 PV (only 14.24 mmol L^{-1}), decreased to almost zero in the subsequent PV (the smallest Al concentration observed in the column effluent was 0.44 mmol L^{-1}), and started to increase towards the value of Al concentration in the input solution only after 20 PV.

The rates of Al precipitation were calculated at different times during leaching in columns 4, 5, 6, 7, 8, 9 and 10 (Table 3). The average rates (in mol s^{-1}, normalized to 1 kg of solution) and their respective standard deviations were also given in Table 3.

3.3.3. Results from applying the stop-flow technique

The stop-flow technique applied at ~65 PV in column 4 and at ~38 and 65 PV in column 6 indicated again nonequilibrium
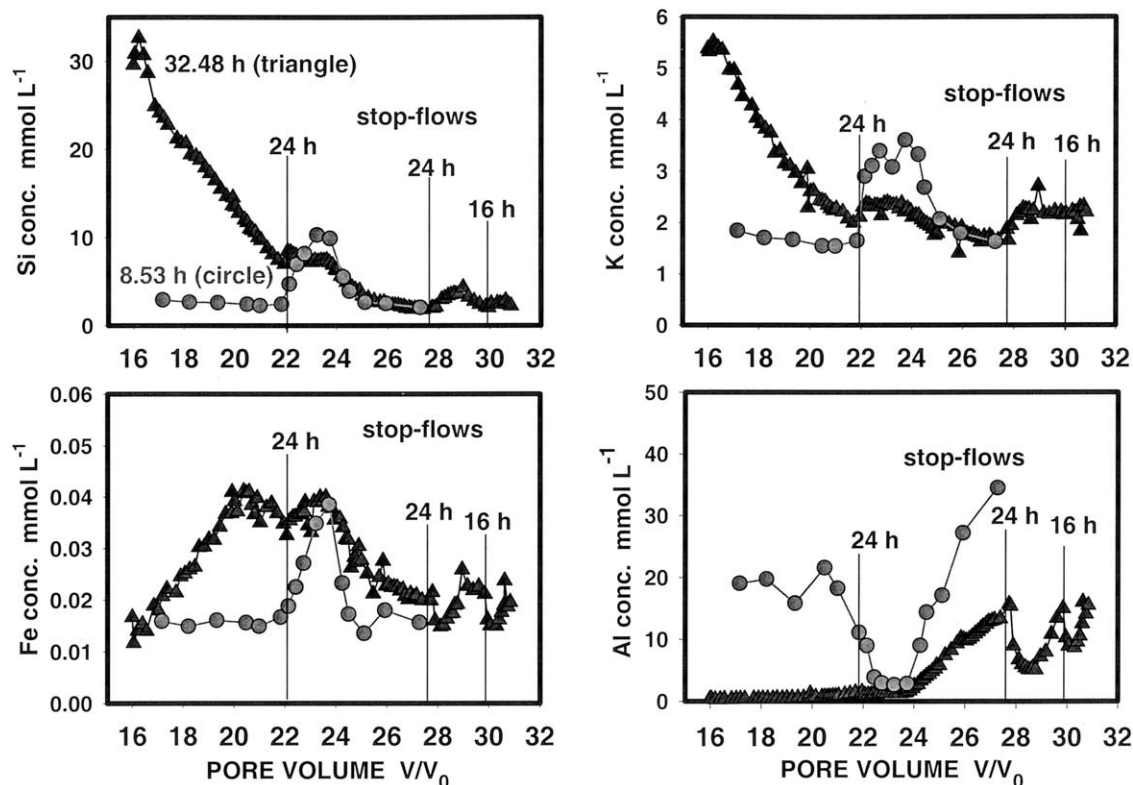
Fig. 4. Changes in Si, Fe, K, and Al concentrations with time in columns 7 and 8. They were leached with 1 mol L^{-1} NaNO$_3$, 1 mol L^{-1} NaOH, 0.055 mol L^{-1} Al(NO$_3$) and 0.192 mmol L^{-1} Cr solutions. Different fluid residence time regimes were applied to these columns (8.53 and 32.48 h, respectively).

conditions. Si concentration in the soil solution increased during these stop-flow events (small graph in Fig. 3). During the stop-flow events at 65 PV, the Si concentration was perturbed more in column 4 (residence time of 4.08 h) than in column 6 (residence time of 8.2 h). It appears that Si concentration is perturbed less in slow columns; for example, Si concentration was only slightly perturbed during the three stop-flow events in column 8 (fluid residence time of 32.48 h), while again it was considerably disturbed in column 7 (fluid residence time of 8.53 h) during the 24 h stop-flow at 22 PV (Fig. 4).

Similar trends to Si were observed for K, but Fe behaved slightly differently, mainly because it underwent almost simultaneous dissolution and precipitation, resulting in relatively low concentrations in column effluents (Figs. 3 and 4). The participation of Al in the formation of the secondary phases was made once again clear during the stop-flow events applied in columns 4, 6, 7 and 8. Al concentrations in the effluents decreased significantly during all stop-flows (Figs. 3 and 4).

3.3.4. Results from modeling

Results from modeling with GMIN showed that the same predominant Al and Si aqueous species as the ones in columns 2 and 3 were present in the effluents of column 4, 5 and 6, with respective fluid residence times of 4.08, 23.56 and 8.20 h. In column 4, the aqueous phase became oversaturated with respect to high OH nitrate-cancrinite and brucite at 1.44 PV and remained oversaturated with respect to cancrinite and goethite at

5.96, 16.02 and 20.74, and 30.02 PV. In column 5, the solution became oversaturated with respect to high OH nitrate-cancrinite, goethite, and brucite (Mg precipitated faster than Ca and Ba) at 1.49 PV. The solution remained oversaturated with respect to high OH nitrate cancrinite and goethite at 5.96, 15.04, 20.19 and 30.18 PV. In column 6, the aqueous phase became oversaturated with respect to high OH nitrate-cancrinite, brucite and portlandite at 1.37 PV, and remained oversaturated with respect to high OH nitrate-cancrinite and goethite at 5.78, 15.14, 20.30 and 30.47 PV.

3.4. The Effect of Aqueous Al on Dissolution and Precipitation

Al was present in significant amounts in the fluids that leaked at the Hanford vadose zone. In addition, Al may have a dual effect on the base-induced mineral dissolution: when it is present in the aqueous phase Al may decrease the OH free concentration at alkaline pH because it forms aluminate ions; at the same time, Al may inhibit base-promoted dissolution. The apparent inhibitory effect of Al on dissolution was clearly demonstrated in the data collected from columns 9 and 10 (Fig. 5). These columns were leached with a 0.165 mol L^{-1} Al, hyperalkaline and saline solution. Less Si, Fe, and K were released in the effluents of column 9 than in the effluents of column 6 (previously presented in Fig. 2, which had a similar fluid residence time but was leached with an alkaline and saline solution that was 0.055 mol L^{-1} in Al.
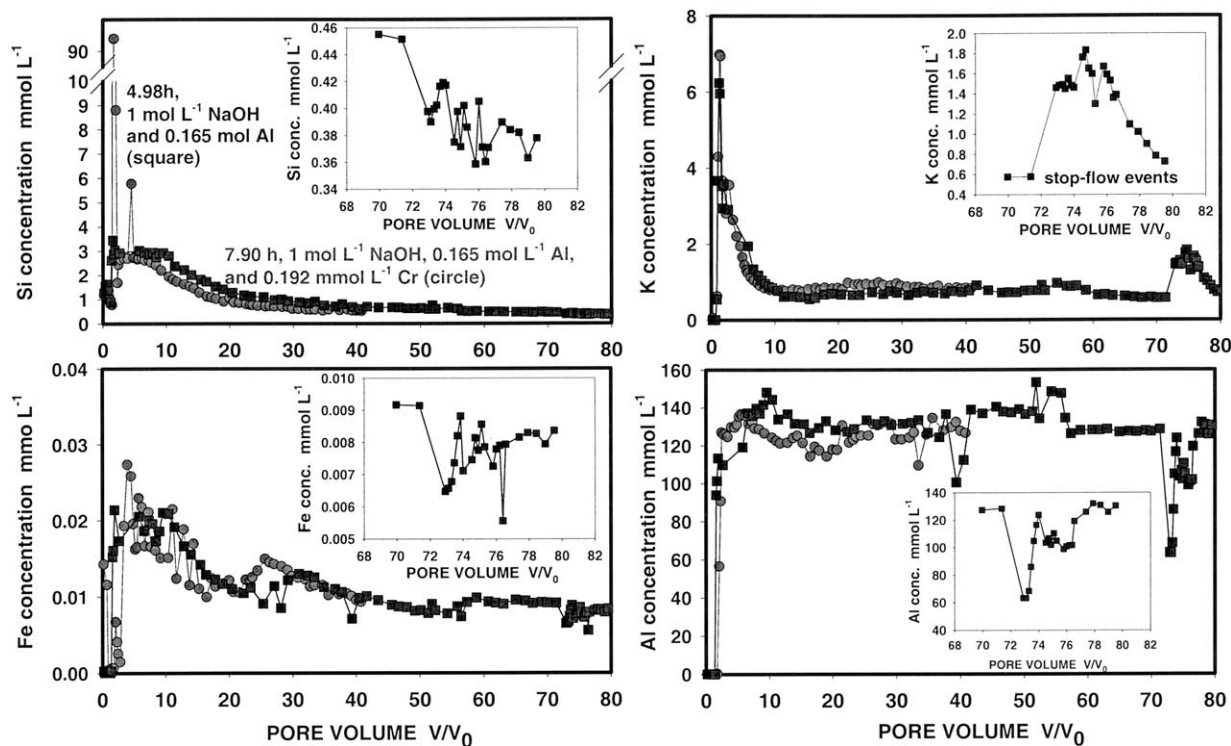
Fig. 5. Changes in Si, Fe, K, and Al concentrations with time in columns 9 and 10. They were leached with 1 mol L^{-1} NaNO$_3$, 1 mol L^{-1} NaOH, and 0.165 mol L^{-1} Al(NO$_3$) solutions that were 1.923 and 0 mmol L^{-1} in Cr, respectively. Different fluid residence time regimes were applied to these columns (7.90 and 4.98 h, respectively).

The initial dissolution rate in column 9 leached with a 0.165 mol L^{-1} Al, alkaline and saline solution was smaller than the rate observed in columns 6 and 2, that were leached with a 0.055 mol L^{-1} Al and Al-free alkaline and saline solutions, respectively (Table 2). The apparent dissolution rates calculated at different times during leaching were also smaller in column 9 than in columns 6 and 2.

The residence time appeared to have no noticeable effect on dissolution and precipitation in the experiments conducted with the 0.165 mol L^{-1} Al solution. Similar trends of changes in Si, K, Fe, and Al concentration with time were observed in columns 9 and 10 (7.90 and 4.98 fluid residence time, respectively) (Fig. 5). The K and Al concentrations significantly increased and decreased, respectively, during the 46, 17, and 17 h stop-flow events at approximately 72, 74.5, and 76 PV in column 10.

The rates of Al precipitation (in mol sec^{-1}, normalized to 1 kg of solution) were calculated at different times during leaching (Table 3). The average rates were similar to those calculated in the other columns that were leached with a 0.055 mol L^{-1} Al solution.

Results from modeling with GMIN indicated that solution was oversaturated with respect to high OH nitrate-cancrinite, goethite and brucite at 1.73 PV, and oversaturated with respect to high OH nitrate cancrinite, goethite, and gibbsite at 5.19, 20.65, and 40.01 PV. The solution was oversaturated with respect to brucite at 5.19 and 40.01 PV.

3.5. The Release of Other Elements in the Effluents

The release of other elements such as Ca, Mg, Ba, and Mn in the column effluents was also followed during these experiments. A peak of Ca, Mg, and Ba concentrations (approximately 0.16, 0.051 and 0.00013 mol L^{-1}, respectively) was observed in the second PV in all columns, and their concentrations remained close to zero for the rest of experiments. Mg was the first one to precipitate out of the saturated solution. A small peak of Mn concentration was observed in the first PVs ($\sim$0.0016 mmol L^{-1} Mn), and Mn concentration remained close to zero afterwards.

Neither the residence time nor the base concentration appeared to have a noticeable effect on the amount of these elements released in the column effluents. However, the concentration maxima of these elements usually observed in the second PV were more intense in column 9 ($\sim$0.24, 0.064 and 0.00029 mol L^{-1}, for Ca, Mg and Ba, respectively), where the free OH concentration was the smallest, because this column was leached with an alkaline and saline solution that was 0.165 mol L^{-1} in Al. This also suggested that these elements were precipitating under extreme alkaline conditions.

3.6. Posttreatment Sediment Analyses

Upon completion of the column experiments SEM and EDS analyses were performed on the sediments that were taken out of the columns. The SEM micrographs showed that the post-
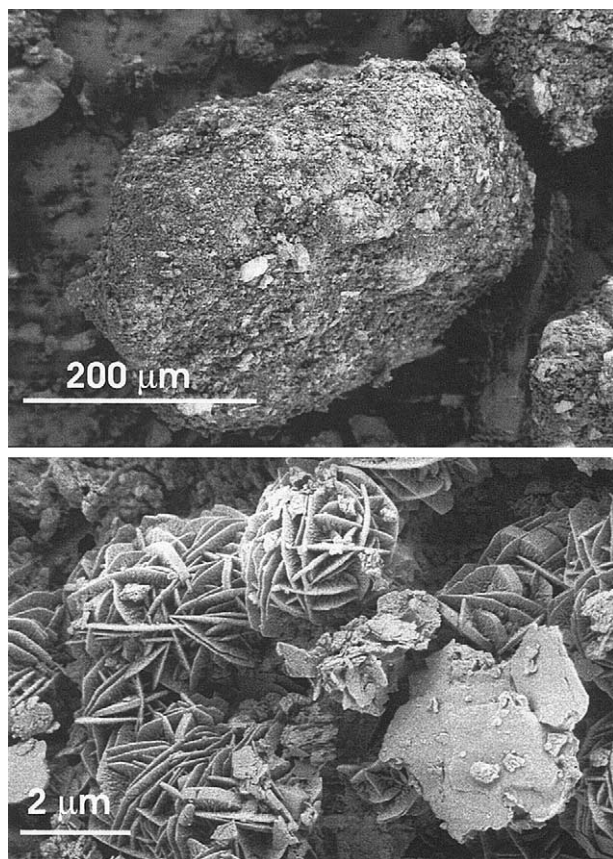
Fig. 6. Scanning electron micrographs taken from the posttreatment sediments of the middle section of column 5 that were leached with the 1 mol L^{-1} $NaNO_3$, 1 mol L^{-1} NaOH, 0.055 mol L^{-1} $Al(NO_3)$, and 1.923 mmol L^{-1} in Cr solution A feldspar particle (top) covered with the cancrinite balls (bottom).

treatment sediments exhibited many of the features noted in the batch experiments (Bickmore et al., 2001; Qafoku et al., 2003a), namely, the formation of the cancrinite balls and rod-like square structures, that most likely were sodalite (Figs. 6, 7 and 8). However, these minerals were more abundant in the posttreatment sediments of these column experiments, probably because of the dynamic nature of these systems where flow continuously refreshed the bathing solution.

The posttreatment analyses of the sediments revealed that, in some cases, secondary minerals fully covered the soil particles in the sediments packed in the columns (Fig. 6, top). The cancrinite balls were clearly visible on the surface of these particles (Fig. 6, bottom). These SEM micrographs were taken from the posttreatment sediments of the middle section of column 5 that was leached with the Al-rich, alkaline and saline solution. Nevertheless, the XRD patterns of the untreated sediments and the sediments taken from the columns at the end of experiments showed no or little differences, probably because their concentrations were close to the XRD detection limit.

The morphology of these Na-rich, alumino-silicate precipitates was significantly affected by the Al and OH concentrations in the aqueous phase. Micrographs presented in Figure 7 were taken from the posttreatment sediments of column 3 that were leached with an Al-free, 4 mol L^{-1} NaOH and 1 mol L^{-1}
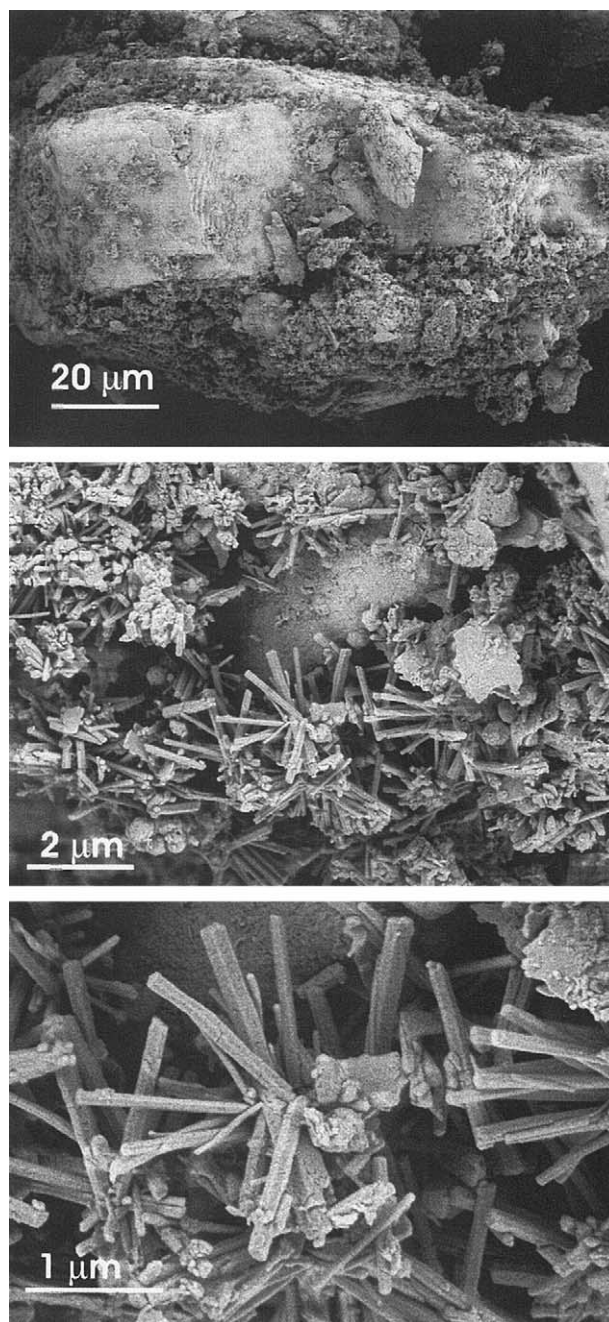

Fig. 7. Scanning electron micrographs taken from the posttreatment sediments of the middle section of column 3 that were leached with the 1 mol L^{-1} $NaNO_3$, 4 mol L^{-1} NaOH, and 0.192 mmol L^{-1} in Cr solution A feldspar particle (top) covered with the rode-like, square crystals (most-probably sodalite).

$NaNO_3$ solution. The precipitates formed in this column had a squared rod-like structure, which most probably was that of sodalite. These crystals were definitely different from the balls formed when an Al-rich, 1 mol L^{-1} NaOH and 1 mol L^{-1} $NaNO_3$ solution was used to leach the columns.

Clear signs of OH attack on mica edges were quite visible in these experiments conducted with the alkaline solutions. The micrographs in Figure 8 were taken in the posttreatment sedi-
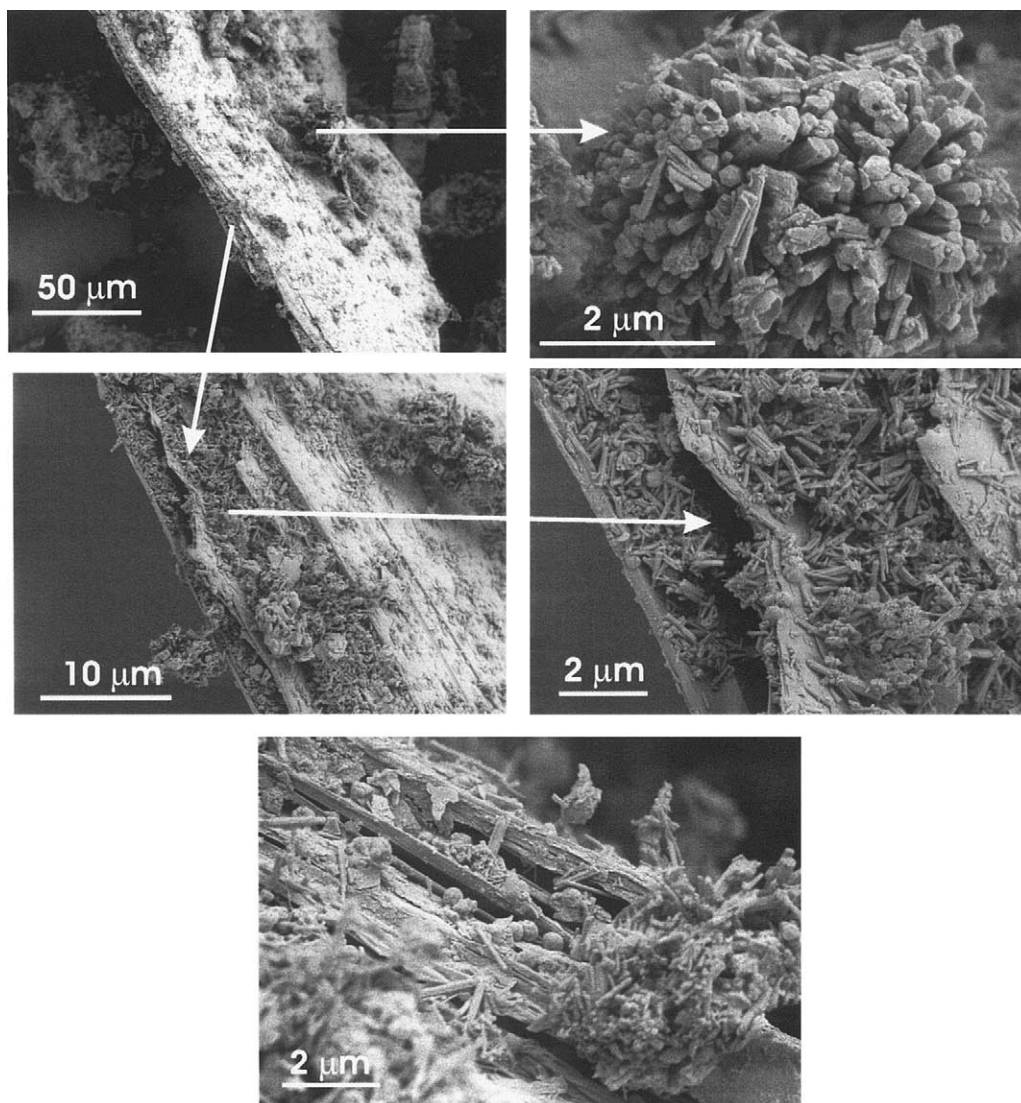
Fig. 8. Scanning electron micrographs taken from the posttreatment sediments of the middle section of column 3 that were leached with the 1 mol L^{-1} NaNO$_3$, 4 mol L^{-1} NaOH, and 0.192 mmol L^{-1} in Cr solution. This figures show the base attack on mica particles in the sediments; the secondary precipitates have filled the opening space created at the edge of the mica particle as a result of the OH attack.

ments of column 3. Openings greater than 2 μm (the distance between mica sheets is usually 1 nm) were observed in this and other mica particles. It is quite interesting to notice, however, that secondary precipitates almost completely covered the edges of mica particles, probably hindering further dissolution.

4. DISCUSSIONS

4.1. The Extent of Base-Induced Dissolution and Subsequent Precipitation

The results from this study clearly show that intense dissolution occurs when sediments are contacted with alkaline and saline solutions. The subsequent precipitation of the secondary phases is also very intense. Although the apparent dissolution rates determined in these column experiments are not in all

cases greater than the ones determined in previous batch studies, the Al precipitation rates were in all cases at least one order of magnitude greater (Qafoku et al., 2003b).

Soil mineral dissolution increases with base concentration and decreases with Al concentration when Al is present in the input solution. Aluminum decreases the free OH concentration in the leaching solution as Al complexes with hydroxides to form the aluminate ion that is the predominant aqueous Al species under hyperalkaline conditions. Aluminate may also inhibit dissolution by competing for surface sites with OH. As it is expected, Cr concentration in the leaching solution has no significant effect on the extent of dissolution and precipitation.

Importantly, the effect of base concentration on dissolution vanishes with time. Eventually the data in Figure 1 present the same concentration profile for Si and K after 15 PV in both columns. The secondary precipitates formed during the exper-

iments covered the surfaces of the soil minerals, making them less vulnerable to further dissolution.

The extent of precipitation of alumino-silicate phases with a molar Si:Al ratio of 1 depends on the availability of Si and Al in the aqueous phase. Precipitation of these phases appears to occur to a much lesser extent in columns leached with an Al-free alkaline solution as compared to other columns leached with Al-rich alkaline solutions. Results from modeling also suggest that Al concentration limits precipitation in columns leached with Al-free solutions. Because dissolution occurs in a much greater extent than precipitation, a significant sediment mass loss is observed in columns leached with Al-free solutions, where precipitation extent is smaller (Table 1).

4.2. The Temporal Dependency of Dissolution and Precipitation

Experiments conducted at different residence times indicate that both dissolution and precipitation have a significant temporal dependency. Most likely the flow affects the form of the reaction, making it kinetically controlled; it appears, however, that this effect is not present in the long residence time columns. In addition, the effect of fluid residence time vanishes with time.

The nonequilibrium conditions in the system are investigated by varying the pore-water flux, i.e., advection, that controls the fluid residence time in the column. The manipulation of the fluid residence time affects solute concentration only if the system is not in equilibrium (Jardine et al., 1998). In our experiments, mineral dissolution is time dependent as evidenced by the release of Si, K, and Fe into the soil solution, which varies with the fluid residence time. We believe this manifestation of fluid time dependency is an indication of spatially controlled nonequilibrium conditions created during reactive transport.

The stop-flow technique, which is more sensitive in identifying the nature of the nonequilibrium conditions, shows that the concentrations of all major elements, such as Si, Fe, K, and Al, are significantly perturbed during the stop-flow events in the fast-flow columns. This is indicative of physical nonequilibrium. It is quite possible that solute diffusion from the smaller to the larger pores is time dependent. The small pores do not participate directly in the advective movement of solution, and diffusion hinders the immediate reach of equilibrium. Diffusion may control not only the rate of the movement of Al from diffusion-constrained pores to the place where Si is generated, but also the rate of Si movement away from the site where it is generated.

Dissolution is faster than precipitation in these column experiments as indicated from the following evidence: 1. The initial dissolution rate measured in the short residence time columns is faster than that measured in the longer residence time columns; 2. The apparent dissolution rates measured before the stop-flow events are faster than those measured during the stop-flow events, when the fluid residence time is further increased; 3. Much more Al is removed from the solution because of precipitation in the long residence time column as compared to the short residence time column. The fluid residence time, therefore, has a greater effect on precipitation than dissolution.
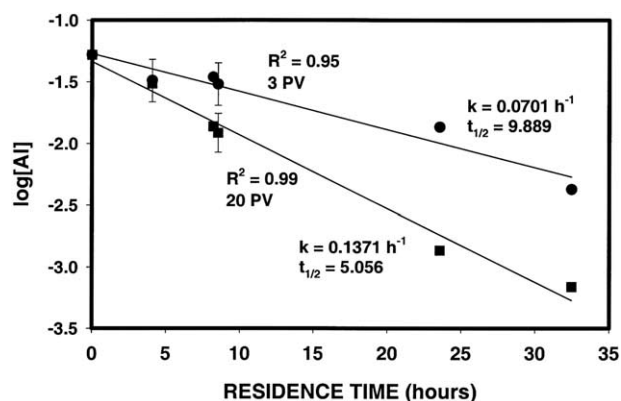

Fig. 9. Al precipitation rate constant and half-life at 3 and 20 pore volume (data from columns 4, 5, 6, 7, and 8).

4.3. The Fate of Si, Al and Fe in the Alkaline and Saline Systems

The fate of Si and Al appear to be closely related in these experiments. In the columns leached with an Al-free alkaline solution, the Al release is much less than Si release upon soil mineral dissolution. Aluminum, in this case, appears to control the rate of Si precipitation in these systems since both these elements coprecipitate in equimolar amounts to form alumino-silicate secondary phases. However, in the columns leached with an Al-rich alkaline solution, Si appears to control the precipitation rate of alumino-silicates, because Al is continuously added into the columns with the injecting solution. This is why the Al leaching profiles are contrary to the Si, Fe, and K profiles in the columns leached with Al-rich alkaline solutions, and these profiles clearly and always indicate Al precipitation. Although the plot of log [Al] vs. time yields a straight line (Fig. 9 with data from columns 4, 5, 6, 7, and 8), which presumably indicates that precipitation follows a first-order kinetics with respect to the aqueous Al concentration, the precipitation in these systems depends only on the Si availability in the aqueous phase, since Al was continuously injected into the columns with the input solution. The precipitation rate constants in these column experiments are much greater than the ones previously determined in batch experiments (Qafoku et al., 2003b).

Iron appears to follow a different precipitation pathway after it is released into the aqueous phase. Modeling results predict Fe precipitation as goethite.

4.4. The Fate of Contaminants in These Systems

The fate of different contaminants during transport in the vadose zone should be closely related to the extent of dissolution that occurs under such extreme alkaline and saline conditions. The release of cations (K, Fe, Ca, Mg, Ba), anions (aluminate and silicates), and redox-sensitive elements (Fe, Mn) upon dissolution of soil minerals should affect the mobility of contaminants present in HLW fluids. For example, Fe(II) released during dissolution of Fe(II)-bearing minerals may reduce contaminants (Cr) (Qafoku et al., 2003c) or radionuclides (Tc, U) via abiotic pathways. Moreover, K, Ca, and Mg may compete for surface adsorption sites with Cs and Sr; the pres-

ence of dissolved Si may result in the complexation of radio-nuclides in solution (Jensen and Choppin, 1996; Moll et al., 1998; Reich et al., 1998); and lastly, Ba may form insoluble complexes with Cr (e.g., $BaCrO_4$). In addition, the newly formed minerals (cancrinite and sodalite) have significant adsorption capacities, and therefore, may drastically retard the contaminant transport in these sediments.

5. CONCLUSIONS

Results from these column experiments indicated that multiple-source, base-induced dissolution and multiple-phase precipitation occurred in the sediments during reactive transport of Al-rich, hyperalkaline and saline fluids. Both dissolution and precipitation were quite intense under extreme conditions of alkalinity and salinity. The precipitation rates calculated in these experiments based on Al removal from the aqueous phase were at least one order of magnitude greater than those determined in previous batch studies.

The changes in the aqueous phase consisted of significant Si, Fe, K, Al, and minor Ca, Mg, Ba, Mn releases into the aqueous phase; a significant Al removal from the injected input solutions was also observed. The release of elements into the aqueous phase as a result of dissolution was time dependent as evidenced by its extent varying with the fluid residence time. Initial Si dissolution rates increased with base concentration, decreased with Al concentration, and decreased with fluid residence time. Aluminum (and Si) precipitation rates varied in the range from 0.44 to 1.07×10^{-6} mol s^{-1}. Aluminum precipitation reaction had an initial rate constant of 0.07 h^{-1}, that increased to 0.137 h^{-1} later in the experiment. These rate constants were much greater than those measured in batch experiments.

The solid phase surface properties were also significantly altered because of dissolution and precipitation. Biotite and feldspars underwent intensive dissolution. The precipitates identified with SEM and suggested from modeling were mainly NO_3-cancrinite. SEM analyses also indicated the formation of sodalite when Al was absent in the leaching solution. Model calculations suggested the formation of brucite, and goethite; the formation of gibbsite was also suggested in the presence of high Al concentrations in the leaching solution.

The aqueous and solid phase transformations, because of base-induced dissolution and subsequent precipitation of secondary phases, should be important determinants of the fate of contaminants and radionuclides in the vadose zone under alkaline and saline conditions.

REFERENCES

Barnes M. C., Addai-Mensah J., and Gerson A. R. (1999a) The mechanism of the sodalite-to-cancrinite phase transformation in the synthetic spent Bayer liquor. *Microporous Mater.* **31,** 287–302.

Barnes M. C., Addai-Mensah J., and Gerson A. R. (1999b) The solubility of sodalite and cancrinite in synthetic spent Bayer liquor. *Colloids Surf. A.* **157,** 101–116.

Bickmore B. R., Nagy K. L., Young J. S., and Drexler J. W. (2001) Nitrate-cancrinite precipitation on quartz sand in simulated Hanford tank solutions. *Environ. Sci. Technol.* **35,** 4481–4486.

Blum A. E. and Stillings L. L. (1995) Feldspar dissolution kinetics. In *Chemical Weathering Rates of Silicate Minerals* **Vol. 31,** (ed. F. A. White and Srivastava R. Brantley), pp. 291–351. Mineralogical Society of America.

Brady P. and Walther J. (1992) Surface-chemistry and silicate dissolution at elevated-temperatures. *Am. J. Sci.* **292 (9),** 639–658.

Brezonik P. L. (1993) *Chemical Kinetics and Process Dynamics in Aquatic Systems.* Lewis Publishers.

Brusseau M. L., Hu Q. H., and Srivastava R. (1997) Using flow interruption to identify factors causing nonideal contaminant transport. *J. Contam. Hydrol.* **14,** 39–54.

Buhl J.-C. and Lons J. (1996) Synthesis and crystal structure of nitrate enclathrated sodalite $Na_{8\ 6}$ $(NO3)_2$. [AlSiO4]. *J. Alloys Compd.* **235,** 41–47.

Buhl J.-C., Stief F., Fechtelkord M., Gesing T. M., Taphorn U., and Taake C. (2000) Synthesis, X-ray diffraction and MAS NMR characteristics of nitrate cancrinite $Na_{7.6}$ $[AlSiO_4.]_6NO_{1.6}$ $(H_2O)_2$. *J. Alloys Compd.* **305,** 93–102.

Chou L. and Wollast R. (1985) Steady-state kinerics and dissolution mechanisms of albite. *Am. J. Sci.* **285,** 963–993.

Devidal J. L., Schott J., and Dandurand J. L. (1997) An experimental study of kaolinite dissolution and precipitation kinetics as a function of chemical affinity and solution composition at 150 degree C, 40 bars, and pH 2, 6. 8, and 7.8. *Geochim. Cosmochim. Acta* **61,** 5165–5186.

Felmy A. R. (1995) GMIN, a computerized chemical equilibrium program using a constrained minimization of the Gibbs free energy: Summary report. In *Chemical Equilibrium and Reaction Models* **Vol. 42** (ed. R. H. Loeppert et al), pp. 377–407, Soil Science Society of America.

Ganor J. and Lasaga A. C. (1998) Simple mechanistic model for inhibition of a dissolution reaction. *Geochim. Cosmochim. Acta* **62,** 1295–1306.

Gautier J. M., Oelkers E. H., and Schott J. (1994) Experimental-study of K-feldspar dissolution rates as a function of chemical affinity at 150 degree C and pH = 9. *Geochim. Cosmochim. Acta* **58,** 4549–4560.

Gerson A. R. and Zheng K. (1997) Bayer process plant scale: transformation of sodalite to cancrinite. *J. Cryst. Growth.* **171,** 209–218.

Hellmann R. (1994) The albite-water system: Part I. The kinetics of dissolution as a function of pH at 100, 200, and 300 degree C. *Geochim. Cosmochim. Acta* **58,** 595–611.

Jardine P. M., O'Brien R., Wilson G. V., and Gwo J. P. (1998) Experimental techniques for confirming and quantifying physical nonequilibrium processes in soils. In *Physical Nonequilibrium in Soils. Modeling and Application* (eds. H. M. Selim and L. Ma), pp. 243–271. Ann Arbor Press.

Jensen M. P. and Choppin G. R. (1996) Complexation of europium(III) by aqueous orthosilicic acid. *Radiochim. Acta* **72,** 143–150.

Jones T. E., Watrous R. A., and Maclean G. T. (2000) Inventory estimates for single-shell tank leaks in S and SX tank farms. RPP-6285 Rev. 0, CH2MHILL Hanford Group, Inc.

Knauss K. G. and Wolery T. J. (1989) Muscovite dissolution kinetics as a function of pH and time at 70 degree C. *Geochim. Cosmochim. Acta* **53,** 1493–1502.

Moll H., Geipel G., Brendler V., Bernhard G., and Nitsche H. (1998) Interaction of uranium(VI) with silicic acid in aqueous solutions studied by time-resolved laser-induced fluorescence spectroscopy (TRLFS). *J. Alloys Compd.* **271,** 765–768.

Oelkers E. H. and Gislason S. R. (2001) The mechanism, rates and consequences of basaltic glass dissolution: I. An experimental study of the dissolution rates of basaltic glass as a function of aqueous Al, Si, and oxalic acid concentration at 25 degree C and pH = 3 and 11. *Geochim. Cosmochim. Acta* **65,** 3671–3681.

Oelkers E. H., Schott J., and Devidal J. L. (1994) The effect of aluminum, pH, and chemical affinity on the rates of aluminosilicate dissolution reactions. *Geochim. Cosmochim. Acta* **58,** 2011–2024.

Park H. and Englezos P. (1999) Thermodynamic modeling of sodium aluminosilicate formation in aqueous alkaline solutions. *Ind. Eng. Chem. Res.* **38,** 4959–4965.

Qafoku N. P., Ainsworth C. C., Szecsody J. E., Bish D. L., Young J. S., McCready D. E., and Qafoku O. S. (2003a) Aluminum effect on dissolution and precipitation under hyperalkaline conditions: II. Solid phase transformations. *J. Environ. Qual.* **32,** 2364–2372.

Qafoku N. P., Ainsworth C. C., Szecsody J. E., and Qafoku O. S. (2003b) Aluminum effect on dissolution and precipitation under hyperalkaline conditions: I. Liquid phase transformations. *J. Environ. Qual.* **32,** 2354–2363.

Qafoku N. P., Ainsworth C. C., Szecsody J. E., and Qafoku O. S. (2003c) The effect of coupled dissolution and redox reactions on Cr(VI)$_{aq}$ attenuation during transport in the Hanford sediments under hyperalkaline conditions. *Environ. Sci. Technol.* **37,** 3640–3646.

Reedy O. C., Jardine P. M., Wilson G. V., and Selim H. M. (1996) Quantifying the diffuse mass transfer of nonreactive solute in columns of fractured saprolite using flow interruption. *Soil Sci. Soc. Am. J.* **60,** 1376–1384.

Reich T., Moll H., Arnold T., Denecke M. A., Henning C., Geipel G., Bernhard G., Nitsche H., Allen P. G., Bucher J. J., Edelstein N. M., and Shuh D. K. (1998) An EXAFS study of uranium(VI) sorption onto silica gel and ferrihydrite. *J. Electron Spectrosc. Relat. Phenom.* **96,** 237–243.

Serne R. J., Schaef H. T., Bjornstad B. N., Williams B. A., Lanigan D. C., Horton D. G., Clayton R. E., LeGore V. L., O'Hara M. J., Brown C. F., Parker K. E., Kutnyakov IV, Serne J. N., Mitroshkov A. V., Last G. V., Smith S. C., Lindenmeier C. W., Zachara J. M. and Burke D. B. (2002) *Characterization of uncontaminated vadose zone sediments from the Hanford reservation: RCRA borehole core samples and composite samples.* PNNL-13757–1, Pacific Northwest National Laboratory.

Walther J. V. (1996) Relation between rates of aluminosilicate mineral dissolution, pH, temperature, and surface charge. *Am. J. Sci.* **296,** 693–728.

Zheng K., Gerson A. R., Addai-Mensah J., and Smart R. S. C. (1997) The influence of sodium carbonate on sodium aluminosilicate crystallization and solubility in sodium aluminate solutions. *J. Cryst. Growth* **171,** 197–208.